

# Supplementary Information for: Narrow heavy-hole cyclotron resonances split by the cubic Rashba spin-orbit interaction in strained germanium quantum wells

M. Failla, M. Myronov, C. Morrison, D. R. Leadley, and J. Lloyd-Hughes\*

*University of Warwick, Department of Physics, Gibbet*

*Hill Road, Coventry, CV4 7AL, United Kingdom.*

(Dated: June 24, 2015)

## Abstract

In this Supplementary Information document we provide: a description of the spectral resolution and detector response deconvolution of the THz-TDS data; layer-by-layer sample details; a summary of the cyclotron resonance of the substrates at elevated temperatures; a description of the time-domain model used, and the equivalence between quantum and classical pictures; and a description of the inclusion of nonparabolicity in the Landau level energy calculation.

## I. SPECTRAL RESOLUTION AND DETECTOR RESPONSE DECONVOLUTION

The discrete Fourier transform (DFT) of the time-domain THz electric field  $E(t)$  over a period  $T$  produces the spectral amplitude  $E(\omega)$  at frequency points separated by  $\Delta f = 1/T$ . Thus the  $n$ th data point in the spectrum is at frequency  $f = n/T$ . Starting from the same time-domain data set and adding (or discarding) a few data points (zero padding or zero removal) thus changes the time window to  $T \pm \delta t$ , and the resolution to  $\Delta f' = 1/(T \pm \delta t)$ . Therefore the  $n$ th data point of the DFT of the truncated/expanded time-signal is at a different frequency than the corresponding DFT of the original signal. Using this approach the frequency-domain data were interpolated.

The deconvolution of the electro-optic crystal's frequency-dependent response is important when analyzing time-domain electric fields obtained from THz-TDS. The propagation velocity mismatch between the THz pulse and the IR gate (detection) beam dominates the response.<sup>1</sup> The response function  $F(\omega)$  of the crystal means that the Fourier transform of the measured signal is  $S(\omega) = F(\omega)E(\omega)$  for incident THz pulse  $E(\omega)$ . For an electro-optic crystal with length  $L$  and propagation vector mismatch  $\Delta k_+ \approx k(\omega) - \omega/v_g$  (where  $v_g$  is the IR gate's group velocity) the response function is given by<sup>1</sup>

$$F(\omega) = \frac{e^{i\Delta k_+ L} - 1}{i\Delta k_+}. \quad (1)$$

The complex THz wavevector  $k(\omega)$  was determined from the known complex refractive index of ZnTe.<sup>1</sup> The incident THz electric field pulse on the detector  $E(t)$  was therefore obtained by taking the inverse Fourier transform of  $S(\omega)/F(\omega)$ .

## II. CYCLOTRON RESONANCE OF SUBSTRATES (P-TYPE AND N-TYPE SILICON)

The structure of the samples is shown in Supplemental Fig. 1(a). To rule out any contribution from the lightly-doped silicon substrates the cyclotron resonances were obtained using THz-TDS. As an example, the transmitted spectral amplitude through SiGe2 at 60 K is shown in Supplemental Fig. 1(b) for  $B = 0, 4$  T. The transmission spectra through each heterostructure were modeled using a stack of dielectrics, including the response of every  $j$ -th layer, each with complex refractive index  $n_j$  and thickness  $L_j$ . For layers with free charges  $n_j$  was determined from the Drude-Lorentz expression for the complex magnetoconductivity  $\sigma(\omega, B) = \sigma_1 + i\sigma_2$ :<sup>2</sup>

$$\sigma(\omega, B) = \sigma_0 \frac{1 - i\omega\tau}{(1 - i\omega\tau)^2 + (\omega_c\tau)^2}, \quad (2)$$

where  $\sigma_0 = pe^2\tau/m^*$ , and for cyclotron frequency  $\omega_c = eB/m^*$ , hole volume density  $p$ , and carrier scattering time  $\tau$ . Good agreement was obtained assuming carriers to reside in the

substrates, with literature values for the electron and hole mass in silicon,<sup>3</sup> as evidenced by the dashed lines in Supplemental Fig. 1(c). The increase in carrier density with temperature allowed an activation energy of  $9 \pm 2$  meV to be obtained for the n-Si substrate (SiGe2). At higher temperatures, and for SiGe1, the CR minima are not distinct due to a reduction in  $\tau$ . At 2 K there is no contribution from the substrates to the cyclotron resonances reported in the main manuscript, as the carriers are frozen out.

### III. TIME-DOMAIN MODEL OF CYCLOTRON RESONANCES

The measured electric field transmitted through the Ge-QWs under a magnetic field  $B$  is given by  $E_{\text{tot},B}(t) = E_0(t) + E_{\text{ind},B}(t)$ , where  $E_0(t) \simeq E_{\text{tot},B=0}(t)$  is the incident electric field. Thus the electric field induced by the CR is  $E_{\text{ind},B}(t) = E_{\text{tot},B}(t) - E_{\text{tot},B=0}(t)$ . The CRs are shown in the time and frequency domains for the two samples in Fig. 2(a,c) and Fig. 2(b,d),

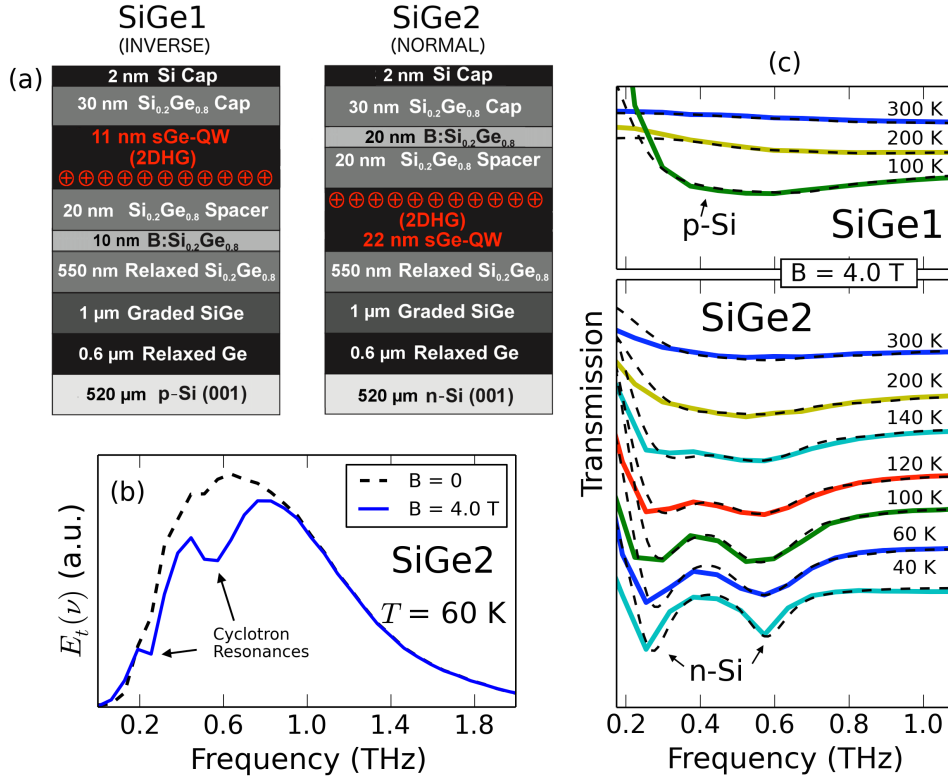


FIG. 1: (a) Structure of samples. (b) Spectral amplitude  $|E(\omega)|$  of THz radiation transmitted through SiGe2 at 60 K and  $B = 0, 4$  T. Two minima in  $E(\omega)$  are evident at  $B = 4$  T (blue line) that are not present at  $B = 0$  (black dashed line). (c) The absolute part of the complex transmission  $|T(\omega, B)| = |E(\omega, B)|/|E(\omega, 0)|$  (colored lines) through the samples is shown at different temperatures for  $B = 4$  T; curves are vertically offset for clarity. Black dashed lines indicate the modeled transmission (see text). Two CR minima are clearly resolved for SiGe2 below 200 K. This is a consequence of the conduction band anisotropy of silicon.<sup>3</sup>

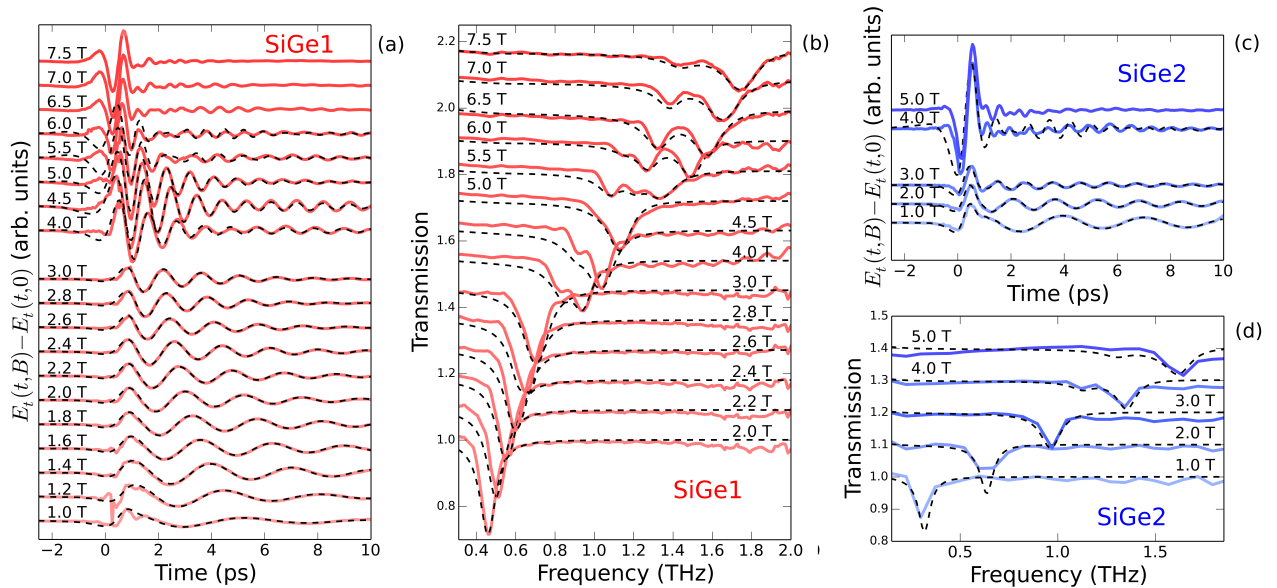


FIG. 2: Time **(a,c)** and frequency **(b,d)** domain cyclotron resonance (CR) at  $T = 2$  K for SiGe1 and SiGe2. The black dashed lines are from time-domain fits as described in the text.

respectively. The dashed black lines are fits obtained as discussed in the following.

In the quantum mechanical view every CR can be seen as a two level system where holes are excited from Landau Level (LL) state  $|1\rangle$  to  $|2\rangle$  with an energy difference defining the cyclotron frequency  $\omega_c = (E_2 - E_1)/\hbar$ . The density matrix formalism describes the dynamics of such a system by solving the Optical Bloch Equations (OBEs), as described for instance in Arikawa *et al.*<sup>4</sup> For short pulses the analytic solutions of the OBEs are provided by perturbation theory which, in the first order, leads to the homogeneous free decay of the diagonal element  $\rho_{12}$  of the density matrix as a result of the interaction with an electric field  $E_0(t)$ :

$$\rho_{12}(t) = e^{-i\omega_c t} \int_{-\infty}^t e^{-(t-t')/\tau} E_0(t') e^{i\omega_c t'} dt'. \quad (3)$$

The two level system defines a macroscopic polarization  $P = 2N\mu_{12}\text{Re}[\rho_{12}]$  where  $\mu_{12}$  is the dipole matrix element between the considered states and  $N$  is the number of two-level systems. The induced electric field  $E_{\text{ind},B}(t) \propto dP/dt$  has frequency  $\omega_c$  and decay rate  $1/\tau$ .

In the classical (Drude) picture holes within the quantum well, with a density  $p_i$  and effective mass  $m_h^*$ , are characterized by the dynamical conductivity:

$$\sigma(t) = [2\pi p e^2 / m_h^*] e^{-t/\tau} \cos \omega_c t. \quad (4)$$

The interaction of the THz field with the hole gas defines an induced current:

$$j_{\text{ind}}(t) = \int_{-\infty}^t E_0(t') \sigma(t-t') dt' = [2\pi p e^2 / m_h^*] \int_{-\infty}^t E_0(t') e^{-(t-t')/\tau} \cos[\omega_c(t-t')] dt', \quad (5)$$

which has a structure similar to Suppl. Eq. (3). In this picture the reemitted THz field  $E_{\text{ind}} \sim$

$dj_{\text{ind}}/dt$  can be written as:<sup>5</sup>

$$E_{\text{ind},B}(t) = [2\pi p e^2 / m_h^*] \sqrt{\omega_c^2 + 1/\tau^2} \times \int_{-\infty}^t E_0(t') e^{-(t-t')/\tau} \cos[\omega_c(t-t')] dt' \quad (6)$$

where the amplitude depends on  $\omega_c$ , the lifetime  $\tau$  and the hole density  $p$ . The experimental CR oscillations at different  $B$  have been fitted by taking into account the sum of different contributions coming from transitions between different states:

$$E_{\text{tot},B}(t) - E_{\text{tot},B=0}(t) = \sum_i A_i \int_{-\infty}^t E_0(t') e^{-(t-t')/\tau_i} \cos[\omega_{c,i}(t-t')] dt'. \quad (7)$$

In Suppl. Fig. 3(a) the CR at 4 T is shown for SiGe1 where a clear beating, between 4 and 6 ps, is resolved. The black dashed line is the fit given by Eqn.7. In this case a good agreement has been obtained with three different contributions having different frequency, lifetime and amplitude and used to model the transmission  $|T(\omega, B)| = |E_{\text{tot},B}(\omega)|/|E_{\text{tot},B=0}(\omega)|$  in the frequency domain (dashed black line in Fig.3(b)). The  $i$ -th contribution to  $|T(\omega, B)|$  is taken into account by defining the total magnetoconductivity as  $\sigma_{\text{tot}}(\omega, B) = \sum_i \sigma_i$ , where  $\sigma_i$  is given by Eqn. 2 with  $\sigma_{i,0} = p_i e^2 \tau_i / m_i^*$ . The depth of valleys in the transmission spectra are proportional to  $p_i$  (related to the amplitude  $A_i$  in the time domain) and  $\tau_i$ , which also characterises their width.

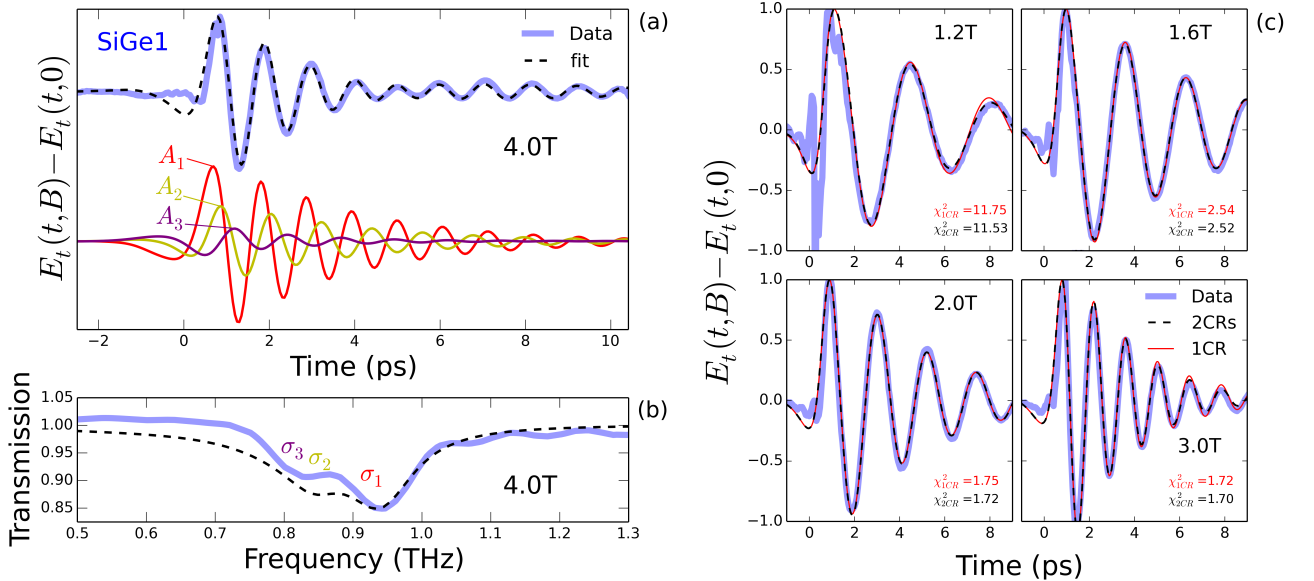


FIG. 3: **(a)** Time-domain  $E(t, B) - E(t, B = 0)$  for SiGe1 at  $B = 4$  T (blue line). The black dashed line is the fit obtained by considering three different transitions each having a different frequency, lifetime, phase and amplitude. **(b)** Transmission in frequency domain at 4 T. The dashed line was obtained using the parameters from the time-domain fit. The amplitudes  $A_1, A_2, A_3$ , as given by the time domain fit, lead to an agreement in the frequency domain, as explained in the text. **(c)** Time domain data and fits using one (red lines) or two CRs (black dashed lines) for SiGe1 (2 K,  $B \leq 3$  T). The agreement of the fits with experimental data is calculated using  $\chi^2 = \sum |y_{\text{data}} - y_{\text{fit}}|^2$ .

The subband dispersion for HH states in the cubic Rashba model leads to a lower spin-up density  $p_{\uparrow}$  than the spin-down density  $p_{\downarrow}$ , since:<sup>6</sup>

$$p_{\downarrow} = \frac{p_s}{2} + \frac{2m_h^*\beta p_s}{\hbar^2\sqrt{2X}}\sqrt{\pi p_s(6-4/X)} \quad ; \quad p_{\uparrow} = \frac{p_s}{2} - \frac{2m_h^*\beta p_s}{\hbar^2\sqrt{2X}}\sqrt{\pi p_s(6-4/X)} \quad (8)$$

where  $X = 1 + \sqrt{1 - 4\pi p_s(2m_h^*\beta/\hbar^2)^2}$ ,  $\beta$  is the cubic Rashba coefficient and  $p_s$  is the total hole density. This is confirmed in the transmission spectra for both samples as well as in Fig. 3(c,d) of the main text where the  $\downarrow\downarrow$  transitions (red lines), which are higher in energy, have a larger density (smaller transmission at resonance). Once the density  $p_{\downarrow}$  was determined such that the modelled  $T|(\omega, B)|$  reaches the same depth as experiment, the hole density  $p_i$  of the  $i$ -th transition was estimated using:

$$p_i = p_{\downarrow} \frac{A_i}{A_{\downarrow}} \sqrt{\frac{\omega_{c,\downarrow}^2 + 1/\tau_{\downarrow}^2}{\omega_{c,i}^2 + 1/\tau_i^2}} \quad (9)$$

where the other parameters are as obtained from the time-domain fits.

Two CRs have been used to fit the CRs in time-domain up to 3 T and three between 4 and 6 T for SiGe1 while, for SiGe2, fits have been obtained by considering two CRs in the whole magnetic field range. For SiGe2 the time-domain oscillations do not show clear, single-frequency decays with exponential envelopes [see Suppl. Fig.2(c)], and these are therefore not possible to fit with just one CR.

For SiGe1 with  $B \leq 3$  T, even if it is not resolved in the frequency domain, two CRs instead of one were considered because of a smaller residual between fit and experiment. In Fig. 3(c) a comparison between fitting with one or two CRs is shown. While the CRs in SiGe1 below 3 T appears, at first glance, to decay exponentially, there is a deviation from single exponential decay that is clearly visible at  $B = 1.2$  T and 3.0 T. Using one CR gave rise to the lowest residual error at  $B = 1.0, 1.4, 1.8$  T. The CR frequencies for spin-up to spin-up and spin-down to spin-down transitions can be similar when LLs overlap, such as sketched in Suppl. Fig. 4. For instance, a time-domain fit at 1.6 T with 2 CRs produces  $\omega_{c,1}/2\pi = 0.3634$  THz and  $\omega_{c,2}/2\pi = 0.3640$  THz (i.e. a difference  $\Delta\omega_c/2\pi = 0.0006$  THz, so effectively one CR), while at 1.2 T a 2 CR fit yields a much larger  $\Delta\omega_c/2\pi = 0.04$  THz.

The CR lifetimes  $\tau$  for spin up-up and spin down-down transitions from the time-domain fits were found to differ by up to about 10%. The partial occupation of the final or initial LL can result in a deviation of  $\Gamma$ , and thus of  $\tau$ , as pictured in Fig. 1(d) of the main text. Since the LL width  $\Gamma$  is thought to be independent of LL index,<sup>7</sup> the average value of  $\tau_{\downarrow}$  and  $\tau_{\uparrow}$  at each  $B$  is reported in Fig. 3(e,f) of the main text.

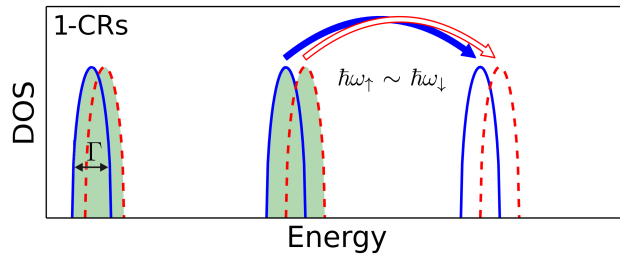


FIG. 4: Density of states (DOS) at low magnetic fields. Because of the overlap between the different Landau levels (LLs) one cyclotron resonance is resolved in the frequency domain.

#### IV. INCLUSION OF NON-PARABOLICITY IN LANDAU LEVEL ENERGIES

The nonparabolicity of the heavy-hole band was taken into account in Eqn. 2 of the main text using the Kane ( $\mathbf{k} \cdot \mathbf{p}$ ) model to include the energy dependence of  $g^*$  and  $m^*$ , according to  $m^*(E) = m_b^*(1 + 2E/E_g)$  and  $g^*(E) = g_0(1 - \alpha_{\text{NP}}E)$ .<sup>8</sup> Here, the energy gap  $E_g$  of the sGe-QW was taken to be 0.7 eV,  $\alpha_{\text{NP}}$  is the nonparabolicity factor and  $E = E_1 + E_{\omega_c, N}^\pm + E_{\text{Zeeman}}^\pm$ . The ground state energy for a rectangular well  $E_1 \propto L_{\text{QW}}^{-2}$  was assumed, and  $E_{\omega_c, N}^\pm + E_{\text{Zeeman}}^\pm$  is the Landau level energy in the parabolic case without a spin-orbit contribution.

---

\* Electronic address: j.lloyd-hughes@warwick.ac.uk

<sup>1</sup> G. Gallot, J. Q. Zhang, R. W. McGowan, T.-I. Jeon, and D. Grischkowsky, *Appl. Phys. Lett.* **74**, 3450 (1999).

<sup>2</sup> J. Lloyd-Hughes, *Journal of Physics D: Applied Physics* **47**, 374006 (2014).

<sup>3</sup> G. Dresselhaus, A. F. Kip, and C. Kittel, *Phys. Rev.* **98**, 368 (1955).

<sup>4</sup> T. Arikawa, X. Wang, D. J. Hilton, J. L. Reno, W. Pan, and J. Kono, *Phys. Rev. B* **84**, 241307 (2011).

<sup>5</sup> D. Some and A. V. Nurmikko, *Appl. Phys. Lett.* **65**, 3377 (1994).

<sup>6</sup> R. Winkler, *Spin-Orbit Coupling Effects in Two-Dimensional Electron and Hole Systems* (Springer-Verlag Berlin Heidelberg, 2003), ISBN 3-540-01187-0.

<sup>7</sup> T. Ando, A. B. Fowler, and F. Stern, *Rev. Mod. Phys.* **54**, 437 (1982).

<sup>8</sup> J. Scriba, A. Wixforth, J. Kotthaus, C. Bolognesi, C. Nguyen, and H. Kroemer, *Solid State Communications* **86**, 633 (1993).